

Explaining the Neuroevolution of Fighting Creatures Through Virtual fMRI

Abstract While interest in artificial neural networks (ANNs) has been renewed by the ubiquitous use of deep learning to solve high-dimensional problems, we are still far from general artificial intelligence. In this article, we address the problem of emergent cognitive capabilities and, more crucially, of their detection, by relying on co-evolving creatures with mutable morphology and neural structure. The former is implemented via both static and mobile structures whose shapes are controlled by cubic splines. The latter uses ESHyperNEAT to discover not only appropriate combinations of connections and weights but also to extrapolate hidden neuron distribution. The creatures integrate low-level perceptions (touch/pain proprioceptors, retina-based vision, frequency-based hearing) to inform their actions. By discovering a functional mapping between individual neurons and specific stimuli, we extract a high-level module-based abstraction of a creature's brain. This drastically simplifies the discovery of relationships between naturally occurring events and their neural implementation. Applying this methodology to creatures resulting from solitary and tag-team co-evolution showed remarkable dynamics such as range-finding and structured communication. Such discovery was made possible by the abstraction provided by the modular ANN which allowed groups of neurons to be viewed as functionally enclosed entities.

Kevin Godin-Dubois*
University of Toulouse, IRIT
CNRS
kevin.dubois@irit.fr

Sylvain Cussat-Blanc
University of Toulouse, IRIT
CNRS
Artificial and Natural Intelligence
Toulouse Institute

Yves Duthen
University of Toulouse, IRIT
CNRS

Keywords
Neuroevolution, competition, emergent communication, co-evolution, ES-HyperNEAT

I Introduction

Artificial neural networks (ANNs), as abstract computational machines, have been used on a large range of problems such as evolutionary robotics (Moriarty & Miikkulainen, 1996), quark mass measurement (Aaltonen et al., 2009), or video game content generation (Stanley et al., 2005). Yet, one of their most fascinating applications is as biomimetic engines that can reproduce key characteristics of the animal brain, thereby paving the way towards its understanding (Treccani, 2020).

However, recent interest in ANNs is focused on applying *deep learning* methodology to similarly abstract problems, from cancer detection (Reshma et al., 2021) to agriculture (Kamilaris & Prenafeta-Boldú, 2018). A complementary approach to such supervised learning tasks is that of neural plasticity (Mouret & Tonelli, 2014). In these situations, the challenge lies not only in devising

* Corresponding author.

the appropriate network topology and connection weights but also, more crucially, solving the learning-to-learn problem (Miconi et al., 2018).

Nonetheless, while current ANNs are capable of reaching better-than-human performance on multiple abstract tasks such as playing Atari games (Mnih et al., 2015), we are still far from general artificial intelligence (GAI). Indeed some authors caution against assigning cognitive capabilities to machine learning agents, arguing that “task-specific performance can [not] be treated as manifestation of General Intelligence” (Kadam & Vaidya, 2021, abstract). In parallel, Zador (2019) argues that biological learning is not the result of clever algorithms but is likely, instead, to depend on a genomic bottleneck responsible for a brain’s rapid learning capacities. Indeed, Zador states that “AI is far from achieving the intelligence of a dog or a mouse, or even of a spider” (p. 2), at least in terms of general intelligence.

A potential solution to this problem is to focus on agents that would autonomously navigate an environment and derive insights into the progressive devising of solutions to the range of problems therein faced. On a long-term time scale, this could lead to the emergence of carbon-/silico-based ecosystems of collaborating humans and robots (Pianca & Santucci, 2022). Such an approach, for instance with neurorobots (Chen et al., 2020), could pay off in a much shorter time-scale by providing two-way progress in Neuroscience and Artificial Intelligence. However, one limiting factor is that of the optimal brain structure: Should we copy the human brain to achieve GAI? What, then, about dogs and spiders?

The research field of neuroevolution provides a way around this problem by taking inspiration not only from the biological brain, but also from biological evolution (Stanley et al., 2019). Indeed, one influential algorithm that jointly tackles the evolution of an ANN’s weight and topology is the *neuroevolution of augmenting topologies* (NEAT; Stanley & Miikkulainen, 2002). Initially, the networks are composed only of input/output neurons, but, through mutational operators, new connections and internal nodes can be created, thereby increasing the complexity of the network. One crucial element of this method is that it is incremental: While the first generations will drastically under-represent the problem’s dimensionality, gradual improvement makes it more likely than not that an efficient trade-off can be reached.

Thanks to its expressive power and relatively straightforward implementation, this methodology has led to a number of derivatives in recent decades (Papavasileiou et al., 2021). One that specifically addresses the scaling problem of the original method is HyperNEAT (Stanley et al., 2009). Indeed, in NEAT each neural component (neurons, axons) is represented by a dedicated gene making it a *direct* encoding. It follows that the genome size is directly proportional to that of the ANN it encodes, making it nigh impossible to deploy on larger networks. Another issue lies in the impossibility to express regular or repeating patterns as any discovery must be made independently. Instead, HyperNEAT evolves a *composite pattern producing network* (CPPN; Stanley, 2007) that serves as an abstraction of natural development. This CPPN then serves as an all-purpose mathematical object that can be queried for specific information. More specifically, if provided with a pair of coordinates p_0, p_1 , the output can be interpreted as a connection weight from a neuron at p_0 to another neuron at p_1 . With such an *indirect* encoding, the genome and network sizes are no longer correlated and the latter can be many orders of magnitude larger than the former. Moreover, by using functions with desirable properties in the CPPN’s internal nodes, it is possible to generate connectivity patterns with repetitions or symmetries.

However, in HyperNEAT, hidden neurons must be explicitly specified by the experimenter, thereby loosing the possibility of exploring emergent topologies. An additional extension, ES-HyperNEAT (Risi & Stanley, 2012), provides an elegant solution by querying the CPPN’s connectivity pattern to discover regions of high informational density. These regions where the pattern is deemed complex enough will be seeded with hidden neurons before any attempt at connection is made. This way, the same genetic component indirectly encodes for both the weights and topology of the resulting ANN while still allowing for larger orders of magnitude. Additionally, the CPPN can be endowed with a second output: the *level of expression* (LEO; Verbancsics & Stanley, 2011), which is a binary value controlling whether or not a given connection should exist. This helps promote

the emergence of modular networks that have been shown instrumental, notably in learning tasks (Ellefse et al., 2015; Tonelli & Mouret, 2013).

To better leverage such a methodology for producing larger-scale ANNs with biomimetic structures, agents should be embedded in complex settings with divergent evolutionary pressures to promote generalist behavior. Indeed, we argue that reaching the intelligence level of, for example, a spider requires grounded neural cognition to study, for instance, the evolutionary dynamics of vision (Cliff & Miller, 1996; Olson et al., 2016) or communication (Jim & Giles, 2000; Kadish et al., 2019; Witkowski & Ikegami, 2016). One direction of particular interest is that of co-evolutionary competition whether in formal settings (Cliff & Miller, 1996; Ito et al., 2013; Sims, 1994) or in ecosystems, especially those consisting of fighting creatures (Miconi, 2008; Pichler & Cañamero, 2008; Turk, 2010), due to multiple, competing evolutionary pressures that favor robustness, first, and peak-performance, second.

In continuity with previous studies, the objective of this investigation is to address the explainability of artificial brain structures in creatures engaged in short bouts. By evolving both the neural network and morphology, the creatures can discover adaptive strategies and, thanks to the co-evolutionary pressure, should develop their brain with sufficient modularity to cope with different combat stages. The challenge is thus to efficiently extract meaningful modeling of internal states in ANNs of up to hundreds of hidden neurons and tens of thousands of connections.

2 Model

The creatures used in this experiment are an expanded version of the elementary circle-like agents from Godin-Dubois et al. (2021b) with three major improvements: (1) they rely on a 3D ANNs, (2) they have a spline-based morphology, and (3) they can develop arm-like manipulators. These allow for a more complex behavioral space that, given the experimental protocol, is instrumental in promoting more convoluted neural dynamics. In the following pages, we explore the various components of the system, with a special emphasis on the morphological elements and the ANN generation procedure. The source code, including scripts and configuration files is available on the corresponding author's github.¹

2.1 Splinoids and Their Genetic Parameters

All creatures are composed of a circular body and optional genetically controlled horn-like constructs based on cubic splines, hence the creatures' name *Splinoids* (Figure 1). These splines can be evolved for various purposes (e.g., offense/defense), with two pairs of splines being statically attached to the central body and two pairs forming primitive arms. Additionally, their morphological parameters also encompass components for specifying vision (e.g., eye position, range), colors, and internal clock speed. Most importantly, they are also endowed with an indirectly encoded 3D ANN using the ES-HyperNEAT paradigm.

The genetic parameters, in increasing order of complexity, are as follows. The first of the elementary parameters is the internal clock speed range which is a pair (s_l, s_u) with $s_l \in [0.1, 1]$ and $s_u \in [1, 2]$, initially both set to 1. These define the lower and upper values that can be reached by an individual's clock. Values above this norm indicate an overdrive with an increased energy consumption (unused in this experiment) in exchange for faster movements. Conversely, values below the norm result in a lower regime but preserve stored resources. Formally, given v , a neural output in $[-1, 1]$ the clock speed $s(v)$ is defined as:

$$s(v) = \begin{cases} 1 + v(1 - s_l) & \text{if } v < 0 \\ 1 + v(s_u - 1) & \text{otherwise} \end{cases} \quad (1)$$

¹ <https://github.com/kgd-al/Splinoids>.

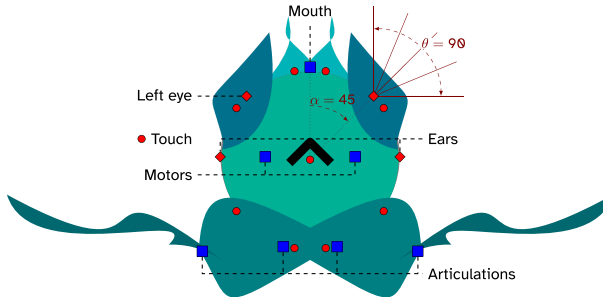


Figure 1. Spiny morphology showing the positions of input neurons (in red) and output neurons (in blue). The black arrow indicates the forward direction. Eyes are placed symmetrically at an angle α on the body surface with a potential relative rotation (none here). The field of vision is θ degrees wide and is subdivided according to the precision parameter (here $p = 2$). Touch sensors (red circles) are placed at every spline's root and at $(0, 0)$ for the body. Articulations (rotational joints) connect forearms, arms, and body. The mouth at the top corresponds to the source of vocalization. For the sake of simplicity, health inputs and clock speed outputs are not displayed as they have no geometrical location.

The second elementary genetic parameter is the color: one for each body part. While essentially simple RGB triplets (in $[0.25, 0.75]^3$), they have a profound impact on the dynamics of the creatures because their visual perception is exclusively color-based (as with the human retina but without light-dependant cells). As such, the various colors of the splines and central body can serve as an identifier of the type of creature encountered without requiring any hard-coded (by the experimenter) recognition scheme. For the purposes of this experiment, the genetic space of all colors has been reduced to green and blue, leaving red aside for health level display (as detailed in section 2.2).

Finally, the vision is composed of four parameters specifying the position of eyes on the body (frontal/lateral), their relative rotation (forward-facing/panoramic), and the width of the field of view. The last parameter concerns the *precision* of the creature's vision and is responsible for the complexity of the visual inputs it can process. For a precision of p , $n = 2p + 1$ retina cells are created for each eye and RGB component. In this experiment p is bounded in $0, \dots, 5$ resulting in retina sizes between 3 and 33 input neurons.² Then, every simulation step, a raycast is performed, starting from the left/right eye location, to detect the color of an eventual colliding object. This information is then used to populate the visual input layer. Note that, due to the 2D nature of the simulation, creatures are prevented from seeing their own body parts. Additionally, a black input is used when no collision is detected, and the arena in which the creatures are embedded is painted in blue.

2.1.1 Spline-Based Morphology

The main morphological component of a Splnoid is the splines of which it is composed. As previously mentioned, there are two different types of splines in the current model. One is static, attached to the creature's body, and serves as an extension of its circular shape. The other is a mobile component subjected to physical forces and is controlled by the creature's ANN. In both cases, however, the generative process is as illustrated in Figure 2 which summarizes the steps by which such a spline, whose parameters are described in Table 1, is interpreted and then sampled to produce a collection of geometrical primitives directly usable by a physics engine.

The process starts by defining the origin of the spline on the body perimeter, that is $p_0 = (\alpha, R)$ with R the creature's radius. We then apply an additional rotation β , to allow for forward- and backward-facing structures, and place the extremity of the spline $p_1 = (\alpha + \beta, R + l)$. By posing $\vec{v} = p_1 - p_0$ and \vec{l} so that $\vec{v} \cdot \vec{l} = 0 \wedge |\vec{v}| = |\vec{l}|$ we define a coordinate system of magnitude proportional to the length of the spline. Thus its control points c_0 and c_1 can be straightforwardly placed

² This restriction aims at limiting the computational cost of vision as well as reducing the subsequent search space of the ANN.

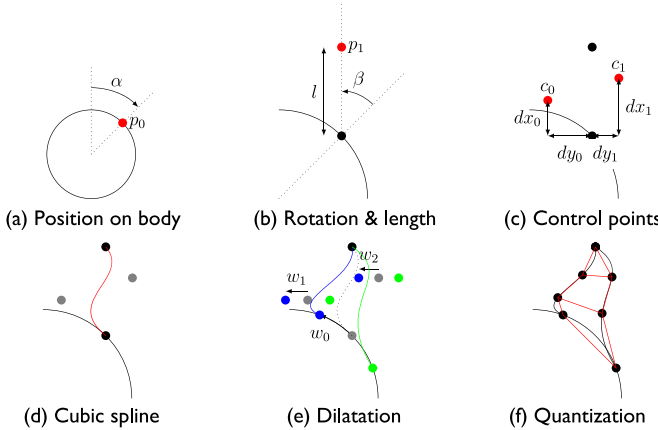


Figure 2. Decoding spline parameters to generate a collection of physical primitives. (a) The spline origin is placed at an angle α on the creature's front. (b) The end point is controlled by an additional rotation β and a length l and forms a coordinate system C . (c) According to C , two control points are placed at position $c_0 = (dx_0, dy_0)$ and $c_1 = (dx_1, dy_1)$. (d) Together with p_0 and p_1 we can define a “mono-dimensional” spline. (e) Three weights (w_0, w_1, w_2) are used to shift the origin and control points in both direction to generate a pair of splines (blue, on the left, and green, on the right). (f) Both splines are sampled, with precision S , generating a small set of elementary shapes. Construction is shown for the right-hand side spline, the other is obtained by axial symmetry. Ranges for all parameters are summarized in Table I.

Table I. Genetic parameters for each spline.

Name	Ranges		Use
	Initial	Mutation	
α		$[0.001, \pi]$	Angular position on body
β	0	$[-\pi, \pi]$	Relative rotation
l	0	$[0, l]$	Spline length
dx_0, dx_1		$[0, l]$	X coordinate of control point
dy_0, dy_1	0	$[-0.5, 0.5]$	Y coordinate of control point
w_0, w_1, w_2	0	$[0, 0.5]$	Dilatation coefficients

Note. The first population is generated with values in the Initial range, whereas subsequent mutations can reach any value in the Mutation range. Parameter names are the same as presented in Figure 2.

according to a longitudinal displacement along \vec{v} (parameters dx_0, dx_1) and transversal, along \vec{t} (parameters dy_0, dy_1). This formulation in terms of relative coordinates allows the spline to maintain an elongated shape as identical values of dy_* will give more or less aligned control points depending on the spline's length.

Once all points have been defined, there is enough information to generate a spline of arbitrary orientation, length, and curvature. However, the objective is to generate 2D surfaces for use in a physics engine and thus requires an additional step: the dilatation. The spline origin p_0 is shifted alongside the body perimeter by an additional weight w_0 thereby producing a new spline root p'_0 to the left of the original. A similar displacement is also applied to the control points, via w_1 and w_2 , resulting in the left-hand side control points c'_0 and c'_1 , respectively. Together these define a new

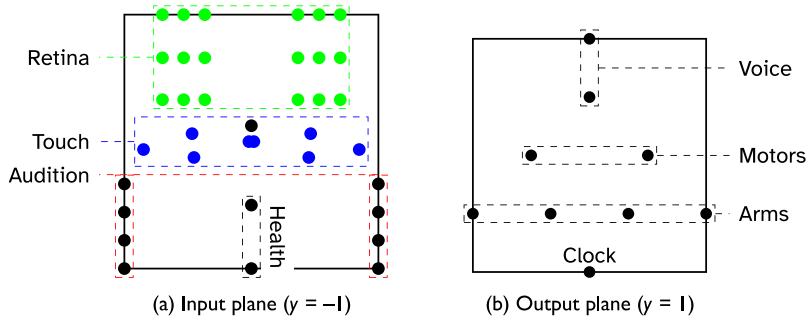


Figure 3. Input (left) and output (right) planes of the ANN's 3D substrate. Most I/O neurons are at fixed positions for every individual (black) while others depend on the creature's morphology. Touch sensors (blue) are placed at the projected origin of the corresponding spline. Input neurons of the retina (green) can vary in position (depending on eye placement) and density (depending on the precision p).

spline, similar to the previous one but shifted in a non-trivial manner. The procedure is repeated with the opposite of each w_0, w_1, w_2 weights, which outputs the points p_{r0}, c_{r0}, c_{r1} used to define a “right-hand side” spline. In both cases p_1 remains unchanged and still corresponds to the end point of each spline. In this manner, we define a mathematical surface enclosed by two splines that share the same endpoint. To transform this surface into a collection of primitive geometrical forms, we simply sample each spline with a specific resolution $S = 4$ and connect the resulting points to form $S - 2$ quadrilaterals and one triangle.³

The rationale behind using splines as the basis for morphological components is that they have enough degrees of freedom to allow for a large panel of shapes. At the same time, as illustrated in Figure 2(f), they are somewhat trivial to transform into elementary shapes that can be used in a physics engine. Thus the creatures can explore a rich phenotypical landscape to better cope with complex situations, most notably physical combat. For future references, we will call the circular part of the creature the *main body*, whereas the *body* will refer to both the main body and its attached, static, splines. Arms will denote the mobile parts of the creature and shall be decomposed into forearms/arms pairs as needed.

2.1.2 Artificial Neural Network and ES-HyperNEAT

As previously stated, a creature's perceptions and actions are encoded via low-level analogical signals, for instance, the intensity of color components in the retina or the magnitude of a motor output (Figure 3). All such signals are processed by a 3D ANN of emergent topology relying on the ES-HyperNeat paradigm. Indeed, as hidden neurons are automatically discovered, we need only specify the position of the input/output neurons on the substrate as detailed hereafter.

All non-hidden neurons are either placed on the input plane ($y = -1$) or the output plane ($y = 1$). The distribution of coordinates is designed to mimic, whenever possible, the geometrical features of the underlying physical counterparts while maximizing separation. With this in mind, retina cells are placed horizontally according to the angular position of each visual ray, thereby linking a specific neuron to a general direction. Arbitrarily, red cells are placed at the top of the retina.

Similarly, touch sensors are positioned with respect to their anchor point on the main body to provide geometrical cues as to where the contact originated from. The sensor associated with the main body itself is placed at $x = 0$ to account for its central position. Auditory sensors are placed on either side of the substrate at $x = -1$ and $x = 1$ for the left and right ear, respectively. These are composed of two types of frequency-dependent perceptions. The uppermost input in each column corresponds to noise involuntarily made by other creatures (for now, only through motion). The

3 Additional tests are performed to split concave shapes into triangles potentially increasing the number of polygons by a factor of two.

remainder perceive communications, that is, voluntary noise productions controlled by two output neurons. The input value for channel i of ear j is given by the formula:

$$\text{audition}(i, j) = \max_{s \in S} (\text{noise}(s, i) - A \text{dist}(\vec{s}, \vec{e}_j)) \quad (2)$$

where S is the set of creatures (itself not included) in auditory range, $\text{noise}(s, i)$ is the volume of sound emitted (voluntarily or not) on channel i , $\text{dist}(\vec{s}, \vec{e}_j)$ is the distance between the emitter and ear j (left or right) of the subject, and A is a scaling constant for the distance-dependent attenuation. In this manner, soundscapes can emerge with different species sharing information on different channels so as to minimize collisions.

Finally, the last two inputs monitor the creatures well-being, with the uppermost providing the normalized health status of the creature between 1 (perfectly healthy) and 0 (dead). The other one is only activated upon receiving damage with a magnitude equal to the normalized health loss (i.e., 0.3 if health drops from 100% to 70%). This allows the creatures to adapt their strategies based on their healthiness, which, as will be detailed in the experimental protocol, can be of help to maximize their efficiency.

Moving onto the output plane, we can quickly address the clock speed whose impact on the creature was already defined in Equation (1). We have two neurons dedicated to voluntary noise production. The output of the neuron at $\zeta = 1$ defines the vocalization volume if said output is greater than 0, thereby helping prevent dubious activation. The other neuron is responsible for the frequency, that is specifying the channel to use. With the current experimental settings, this maps $[-1, -\frac{1}{3}]$, $[-\frac{1}{3}, \frac{1}{3}]$, and $[\frac{1}{3}, 1]$ to channels 1 to 3, respectively.

Motor outputs are directly transformed into impulses of corresponding magnitude applied at $(-R/2, 0)$ and $(R/2, 0)$ in local coordinates. This way, the creatures behave like tanks via forward and backward motion, on-the-spot rotation, and all intermediates. In a similar manner, the output for each articulation allows an individual fine control over the relative positions of each portion of its arms by, once more, applying impulses. Positive values rotate the connected object counter-clockwise and oppositely for negative values.

The CPPN function set for this experiment is as follows: absolute value, bimodal sigmoid, gaussian, identity, sin, and step. As we rely on 3D ANNs, it possesses six inputs for the coordinates of the pre- and post-synaptic neurons as well as an additional input directly providing the distance between them. Besides the weight output, the CPPN is also queried on whether or not to express each connection (LEO). It further produces per-neuron bias on a third output by providing the position of the neuron of interest as the first coordinate and arbitrarily setting the second to $(0, 0, 0)$. ES-HyperNEAT is configured for a minimal and maximal division depth of 2 and 3, respectively with 10 hidden neuron discovery substeps (iterations) and thresholds of 0.3, 0.3, 0.15 for the division, variance, and band thresholds, respectively.

2.2 Physics and Combat

All the morphological and neurological components presented in the previous section interact with one another to generate high-level, observable, behaviors most of which are controlled by the physics engine.⁴ While, we have already covered vision (through ray-casting) and motion (via non-centered impulses), we still have to detail the manner in which creatures can damage one another.

First, let us consider the articulations linking either an arm to the body or an arm to the forearm. As previously illustrated, in Figure 1, we have two such articulations on either side of the creature. Functionally, these are controlled through impulses emitted by the physical engine whose magnitude is directly proportional to the corresponding neural output. They are implemented as rotational

⁴ Implemented as an extension of the Box2D engine: <https://github.com/erincatto/box2d>.

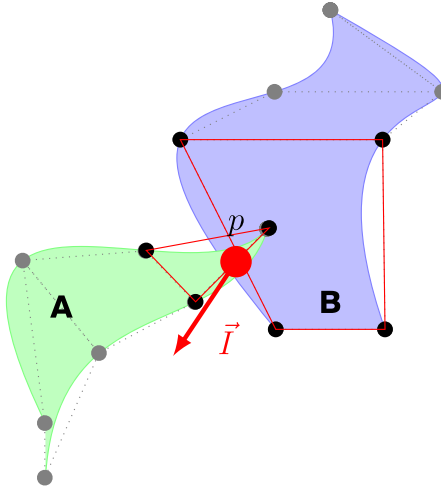


Figure 4. Processing collisions between elementary shapes. One component (red triangle) of spline A collides with another (red quadrilateral) of spline B. The physics engine determines an efficient collision point p and the minimal impulse \vec{I} to separate both shapes which are used to compute inflicted damage.

joints which oppose movement if said output is null and have a maximal torque threshold to limit the speed of massive structures. Moreover, to ensure a physically stable morphology, each joint is constrained to maintain a maximal relative distance between the two objects it connects. Violating this constraint results in both the articulation and the orphaned object(s) to be removed from the simulation. This ensures that (a) non-viable combinations of huge forearms and tiny arms cannot be exploited by evolution, and (b) articulations are not indestructible, thereby reducing the chances of soft-locking.

The procedure for assigning health damage from a collision relies on the physics engine's elementary shapes (triangles and quadrilaterals for the splines, and circle for the body), as illustrated in Figure 4 for a simple spline-spline collision. The prominent variable is \vec{I} , the impulse vector computed by the physics engine to determine the most efficient way to solve the interpenetration. This mass-dependent impulse is then applied to push both objects, thereby maintaining the validity of the system. However, our principal concern is how to transform such interpenetration into health damage, which requires additional information. Given \vec{A}_0 and \vec{B}_0 the velocities of objects A and B *before* the collision and \vec{A}_1, \vec{B}_1 their velocities *afterward*, we define the health damage $damage(\mathcal{A})$ incurred by A as:

$$\rho(\mathcal{A}) = \begin{cases} 0.25 & \text{if } \mathcal{A} \text{ is the main body} \\ 1 & \text{otherwise} \end{cases} \quad (3)$$

$$\Delta V(\vec{v}_0, \vec{v}_1) = \max(0, |\vec{v}_1| - |\vec{v}_0|)^2 \quad (4)$$

$$damage(\mathcal{A}) = \gamma \frac{\rho(\mathcal{A})}{\rho(\mathcal{A}) + \rho(B)} (\Delta V(\vec{A}_0, \vec{A}_1) + \Delta V(\vec{B}_0, \vec{B}_1)) |\vec{I}| \quad (5)$$

where γ is a scaling factor and $\rho(\mathcal{A})$ takes into consideration the density of object \mathcal{A} . More precisely, Splinoids have an advantage in fighting through splines due to a differential in mass between their soft bodies (density 1) and horns (density 2). This is further magnified by ρ so that body-body and

spline-spline confrontations result in equally shared damages, whereas, in spline-body collisions, 80% of the damage is incurred by the vulnerable “fleshy” object. Note that this increased density also has an impact on mass, implying that splines weigh twice as much as a body, for equal surface area. However, this does not have an impact on the object’s health, which is strictly equal to said surface area: 0.25π for bodies and the sum of each elementary shape’s mass for splines.

In this experiment, the healthiness of every body part (main, splines, arms) is color-coded on the red channel. This way creatures can extrapolate the amount of damage sustained by a given object simply by taking into consideration the magnitude of this component.

3 Experiment

With creatures now capable of physical confrontation, we can move onto more complex evolutionary scenarios than simple foraging. More precisely this article is devoted to a co-evolutionary arms race with a straightforward objective: reducing the opponent(s) health to zero. As with previous publications, this evolutionary fitness is expected to promote specific features in the unconstrained ANN, which will illuminate how information is amalgamated and then processed.

3.1 Evolutionary Protocol and Fitness

First, we define the mk fitness, given A and B the normalized *main body* health of the evaluated Splinoid and its opponent, respectively, as:

$$mk(A, B) = \begin{cases} 2 & \text{if } A > 0 \wedge B = 0 \\ -2 & \text{if } A = 0 \wedge B > 0 \\ -B + A & \text{if } A < 1 \wedge B < 1 \\ -3 - d & \text{otherwise} \end{cases} \quad (6)$$

with d the distance between both individuals at the end of the evaluation. The last case corresponds to a failed competition where the creatures are still at full health. Thus, an incentive is provided to discourage strictly avoidance strategies. The general case $-B + A$ rewards any damage inflicted by the subject to its opponent while penalizing the alternative. Finally, we encourage all-in behavior through a markedly higher fitness when the opponent is killed, the counterpart being that having its health reduced to zero incurs a similarly high penalty. Note that the health status of splines is not considered, allowing sacrifice of parts of the morphology to inflict or prevent damage. Each evaluation is 20 seconds long (500 time steps), leaving enough time for each individual to move around and inflict multiple hits. When the time limit is reached or if a creature is downed or immobile, the evaluation is stopped and the score of the subject is computed.

To study the potential emergence of cooperation, two configurations are employed: 1v1 and 2v2. In the first case, the arena is 5×5 meters and the competitors are placed 1 meter away from each other (Figure 5(a)). Both are facing each other and are close enough to see and hear one another immediately. In the second case, the arena has twice the surface area to accommodate the increased number of competitors. For simplicity’s sake, team members are clones, thus having identical morphology and neural controller. However, their initial positions lead to different inputs, thereby allowing each individual to know its relative placement. Furthermore, in 2v2 competitions, the health values A and B from Equation 6 refer to the *minimum* of each team further promoting ruthlessness. That is, killing one enemy is enough to ensure dominance but, conversely, losing a teammate equals defeat. Hereafter we will refer, when appropriate, to 1v1 and 2v2 cases as T1 and T2, respectively.

$$A = \min_{s \in \text{team}} \text{health}(s) \quad (7)$$

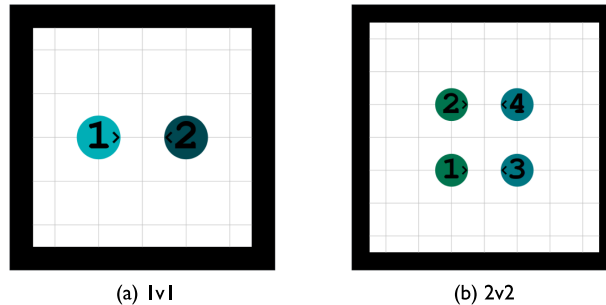


Figure 5. Initial configuration for the two different team sizes. (a) The subject (1) and its opponent (2) are 1 meter away from one another. (b) Tag teams, composed of identical clones, are separated by the same distance but are placed in a larger arena (twice the area).

From these two configurations, we expect different types of interactions to emerge with an approach more focused on collaboration in the 2v2 case. However, another dimension is also investigated in this article: (mild) generalization. This takes the form of having either two or three co-evolving populations, in which case every individual's fighting capabilities are evaluated against either one or two opponents. This opponent is the previous generation's champion of the competing population(s), except for the very first generation where it is taken randomly. Thus, in the two populations case (hereafter reduced to P2), it is enough to find a minimal strategy for inflicting damage upon a probably well-known opponent. However, with three co-evolving populations (P3) one must be proficient against two types of foes with potentially radically different strategies. Moreover, to apply the appropriate response to an opponent, one must know which type one is facing, which should promote better feature-recognition capabilities. The fitness is, again, slightly altered so that failure is more strongly weighted than success:

$$mk(A, B, C) = \frac{1}{3} \max(mk(A, B), mk(A, C)) + \frac{2}{3} \min(mk(A, B), mk(A, C)) \quad (8)$$

All in all, this results in four types of evolutionary strategies:

T1P2 Base case: atomic teams and only two competing populations,

T2P2 Teams of two,

T1P3 Three competing populations, and

T2P3 Teams of two, three competing populations.

We performed 24 and 16 runs for T*P2 and T*P3, respectively, resulting in 48 champions for all alternatives. All runs last for 2,000 generations and have a population size of 200 with only mutation-based reproductions and one elite conserved across generations. A novelty metric was also used based, in part, on the creature's morphological component's masses, and individuals were chosen via a Pareto front selection. The evolutionary part of this experiment relies on the GAGA library.⁵

Creatures start with a minimalist genome to limit the risks of premature convergence. That is all splines start with most parameters at zero and thus have no impact on the morphology. Similarly, the initial neural network is derived from a very simple CPPN where every input has a 50/50 chance to be connected to an output, with no internal nodes. This way, any improvement observed in latter generations can be attributed to the impact of evolutionary constraints, namely the opponent(s).

⁵ <https://github.com/disset/gaga>.

3.2 Neural Evaluation

As in previous publications (Godin-Dubois et al., 2021a, b), the objective of the experiment is to investigate the emergence of neural structures in response to perceived classes of stimuli. As such, we use a similar approach for the extraction of behavioral clusters inspired by functional magnetic resonance imaging (fMRI). In short, we subject an individual to a specific stimulus for predefined periods of time and note which neurons respond to it. We can then provide a functional mapping of the creature's brain according the studied criteria, thereby reducing the observable complexity of the network. Here, the use of a 3D ANN makes it of even more prominent interest due to the inherent problems added by this third dimension.

Indeed, whether through analysis of the neural pathways of the animal brain (Ledoux, 1998), the use of identified key cerebral regions to produce plausible artificial behavior (de Freitas et al., 2007; Delgado-Mata et al., 2007; Lotfi & Akbarzadeh-T., 2014), or mathematical approaches (Broekens et al., 2015), numerous methodologies have been devised to understand and mimic the biological brain. We argue, however, that all such approaches rely on the initial bias of our evolutionary history, whereas artificial intelligence, explainable or not, could span from unexpected convergence of different factors. Especially with the highly scalable and geometry-aware ANNs produced by ES-HyperNEAT, we can expect the resulting brains to exhibit natural patterns such as bilateral symmetry or partitions.

As introduced above, to accurately detect functional mapping between stimuli and neurons, we subject an individual to a controlled condition of oscillating stimuli. In this experiment, we investigate modular clustering from three different angles: pain, discrimination, and communication. In all cases, the conditions are identical with only the type of applied stimulus changing throughout the evolution. Each individual is thus pinned (no movement allowed) to the center of an empty, wall-less arena. To ensure that even laterally placed eyes can detect the target object, we force the subject's orientation to $\theta(t) = \sin(2\pi t)\pi/4$ with $t \in [0, 1]$ corresponding to the relative duration of an exposition period. We expose the individual to the given stimulus for 4 simulated seconds (100 time steps), followed by a relaxation of equal duration without said stimulus. This pattern is repeated 3 times resulting in 300 observations with and without the stimulus, thereby producing a data set of differential activation. We then compare, for each neuron, their states depending on either the

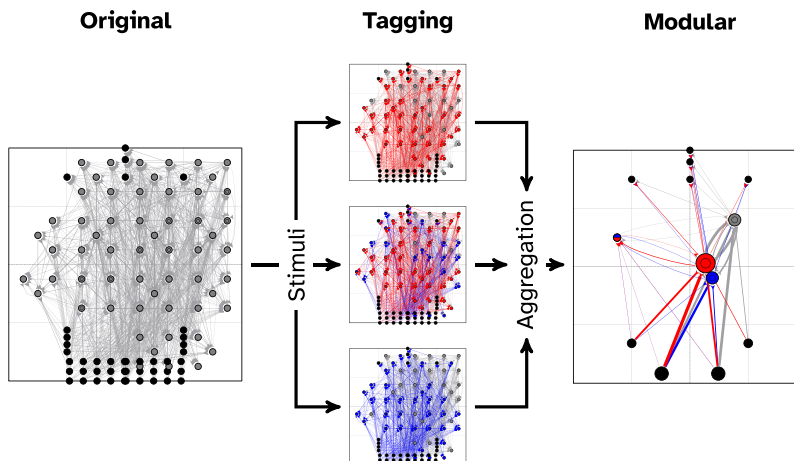


Figure 6. Producing a modular ANN based on individual neurons' activity patterns in canonical conditions. For ease of reading, illustrating graphs use an older, 2D substrate. Left: a black box of hidden neurons and dense connections. Middle: we subject the creature to “simple” stimuli and note which neurons respond. Right: per-neuron response is aggregated, depending on the type of stimuli, to produce functional modules, that is, groups of neurons that have similar dynamics in similar circumstances. The geometrical position is obtained by averaging individual neuron position. All z components are ignored, and slight shifts are applied to limit overlap.

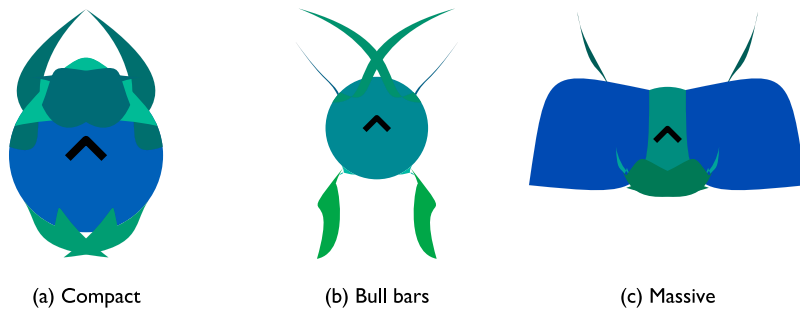


Figure 7. Morphological sample from the 192 resulting champions.

presence or absence of the studied stimulus via a one-sided Mann-Whitney test.⁶ All neurons that are found having a statistically different dynamic are then tagged as monitoring this stimulus, which, when rendered with arbitrary colors, allows for the visualization of functional areas (Figure 6).

Depending on the objectives of the given evaluation, the ANN is subjected to different classes of stimuli that are then aggregated. Subsequently, we generate modules from similar neurons depending on the associated flags. If these are null, a default grey module is generated corresponding to the neurons unrelated to the specific scenario. Those who only responded to a single stimuli are rendered with a single color, whereas those with multiple flags use a combination indicating their different functional responsibilities. To show the number of aggregated items, module sizes are linearly scaled according to the number of neurons they abstract, and inter-module connections are logarithmically scaled based on the number and weights of the underlying axons. Thanks to this procedure, we can observe the dynamics of an arbitrarily complex ANN via the prism of specific stimuli. Indeed, the underlying network is left unchanged: The modular version merely provides the necessary perspective to monitor emergent higher-level behavior.

4 Morphology and Behavior

After 2,000 generations of morphological and neural evolution, the 192 resulting champions have much diverged from their smooth, near-brainless original ancestors. For reference, we provide, in Figure 7, three individuals that inhabit different regions of the morphological space. On the left, the creature has a protective “crown” on the front to better deflect forward attacks and a lighter similar defense at the rear. Its rest morphology is very compact with its two arms almost completely enclosed by the body. However, once active it quickly reaches out using its forearms as flails.

Another strategy, embodied by the individual in Figure 7(b) uses both “bull bars” to maintain distance from the enemy, and rapid back-and-forth motion to maximize damage and prevent deadlocks. Unlike the previous example, its arms are extremely small and located at the rear while the forearms have a blade-like quality that allows for longer reach without sacrificing much speed. Oppositely, other individuals chose a much more ponderous approach based on heavy splines for unbreakable protection. The creature in Figure 7(c) combines both small out-reaching splines with super-heavy fortifications. In this case, most damage is still inflicted by the posterior arms due to its extremely limited speed precluding any charge attempt. Naturally, this sample only offers a very partial view of the morphological and behavioral spaces (e.g., swimming motion, battering arms, tracking). To solve the former, we provide in Supplementary Material A a complete collection of the 192 champions, as well as videos on the corresponding author’s vimeo page.⁷ (Please find supplemental material for this article online here: https://doi.org/10.1162/arl_a_00389).

⁶ This is with a corrected p value threshold taking into consideration the size of the network.

⁷ <https://vimeo.com/showcase/9613894>.

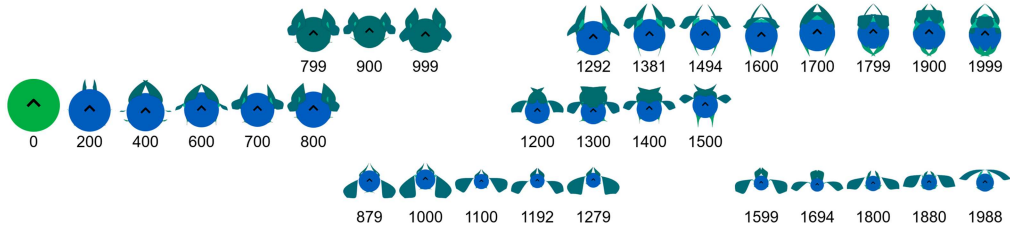


Figure 8. Morphological evolution of the creature from Figure 7(a). After an initial period of straightforward increase in complexity (generations 0–800), multiple lineages cohabit in the population right until the end. While images are down-scaled as needed, all main bodies have the same radius.

To better understand the evolutionary dynamics induced by the experimental protocol, we highlight, in Figure 8, the gradual increase in complexity of the individual in Figure 7(a). At generation 0, the initial morphology is a featureless circular body of arbitrary color, quickly replaced in a few hundred generations by a dominant blue hue. At the same time, the creature’s splines are becoming more and more prominent, with a distinctively different color (gen. 800). Around this mark, however, the joint effect of the novelty metric, which favors originality, and the fluid nature of the fitness landscape results in multiple evolutionary tracks coexisting in the same population (gen. 879–900). Such a trend persists for all following generations, with the most successful individuals emerging alternatively from the concurrent subpopulations, depending on the characteristics of the opponent they faced.

Furthermore, while some alternatives do not persist for more than a few hundred generations (e.g., 799–999 upper row and 1,200–1,500 middle row), others perform well enough to remain in the general population, allowing for a potential resurgence (e.g., 1,279–1,599 lower row). In the context of such a co-evolutionary experiment, this repertoire of alternative morphological and behavioral solutions allows for more flexibility in the selection process as each new strategy exhibited by an opponent is more likely to have a plausible countermove. Indeed, the situation illustrated here, for the physical component, is just as strongly pronounced for the ANN with correspondingly large reservoirs of behavioral trends.

From a broader perspective, we observe limited differences between the four types of evolution despite their variations in environmental complexity and computational cost. Indeed, one of our initial hypotheses is that, naturally, more complex environments should lead to more complex brains. If we equate “complex” to “big,” the answer is clearly negative, as illustrated by the distribution in Figure 9(a), which accounts for the number of hidden nodes. No statistical differences were found

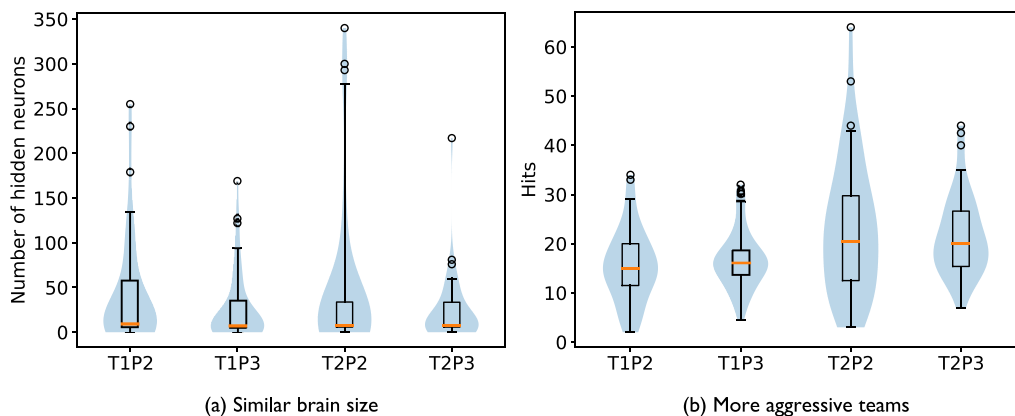


Figure 9. Overview of the distribution of two key emergent characteristics: brain size and aggressiveness. Left, all evolution types have similar numbers of hidden neurons. Right, teams of two score significantly more hits on their opponents than isolated individuals.

Table 2. Stimuli applied to an individual in the first type of evaluation.

Type	Name	Target	Value
H	Health	Body health	0.1
I	Pain	Neuron (0, -1, -1)	0.9
T	Touch	Body touch sensor	1

Note. Stimuli I and H correspond to different, objective, damage inputs. Stimulus T signals the creature that its central body is in contact with something. The rightmost column indicates the values perceived by the individual.

between the groups, thereby rejecting this form of the hypothesis. If, instead, we look at “complex” as “more efficient” we can find that tag teams hit consistently more often their opponents than solitary individuals. This difference was found statistically significant for all T2 variants against all T1 ($p < 0.025$). Surprisingly, another strong difference was found in terms of upper clock speed between the single- and two-opponent cases, with both P2 types being significantly lower than P3 types, indicating better sprint capabilities.

5 Functional Analysis

While the evolved creatures demonstrated non-trivial solutions to the literal arms race both in terms of morphology and behavior, the objective of this experiment lies more on its neural instantiation. Brains of different sizes have been obtained, with outliers ranging from no internal neurons⁸ to about 60% of the maximal density. The purpose of the following sections is to observe the solutions previously described via the prism of functional clusters. In effect, we will address the following questions:

- Can the mapping from inputs to internal states be explained without any need for in-depth, per-neuron analysis?
- What is the impact of these internal states on the outputs?
- Can we extract a functional high-level map of a creature’s brain?

5.1 Evaluation I: Pain

The first type of perception investigated relies on proprioceptors monitoring the creatures’ healthiness and contacts. Table 2 summarizes the three types of stimuli applied to an individual. The first, Health (H) emulates the creature receiving massive, sudden damage by dropping its body health down to 10%. This is performed in the “normal” way, that is, by applying an injury in the same manner that collision with a foreign object would cause. We can contrast this with the I stimulus where, instead, a specific neuron is set to the target value of 0.9. Such a manipulation is likely to produce some artifacts due to the unexpected nature of the changes and inconsistency with the creatures’ global state. Indeed while stimulus H induces both long- and short-term pain by indirectly stimulating both related neurons, stimulus I only acts on one neural input. Similarly, when moving on to the neutral phase, restoring the health level to 100% is, again, an unexpected event as creatures, in this experiment, have no regenerative capabilities and thus have never experienced such input dynamic. Finally, stimulus T is much more mundane as it only consists in activating the neuron responsible for detecting collisions with the main body. In this case, any combination may

⁸ 1 for TIP2, TIP3, T2P3 and 4 for T2P2.

Table 3. Proportion (%) of champions, in each run type, that exhibited pain-related modules.

Type	Touch	Health	Pain	Type	I+	2+	3
TIP2	45.83	37.50	27.08	TIP2	62.50	27.08	20.83
TIP3	33.33	27.08	20.83	TIP3	47.92	25.00	8.33
T2P2	29.17	20.83	14.58	T2P2	43.75	18.75	2.08
T2P3	35.42	29.17	27.08	T2P3	52.08	29.17	10.42

(a) Stimulus specific

(b) Multimodular

Note. The overall response is moderate-to-low with TIP2 and T2P3 coming out on top in both cases. (a) Pain processing is relatively less frequent compared to touch. (b) Individuals frequently express one type of module but only TIP2 does so consistently for all three modules.

have been experienced throughout each creature's evolutionary history and should not introduce undue bias.

Individuals responded moderately to all stimuli with a notably stronger reaction to touch, as can be seen in Table 3(a). Conversely, the stimuli for which the least number of clusters was found is I, which might be explained by its relative short-term activation in "natural" conditions. In turn, individuals may have either preferred to allocate cognitive resources to more relevant tasks or they may have simply failed to capitalize on random emergence.

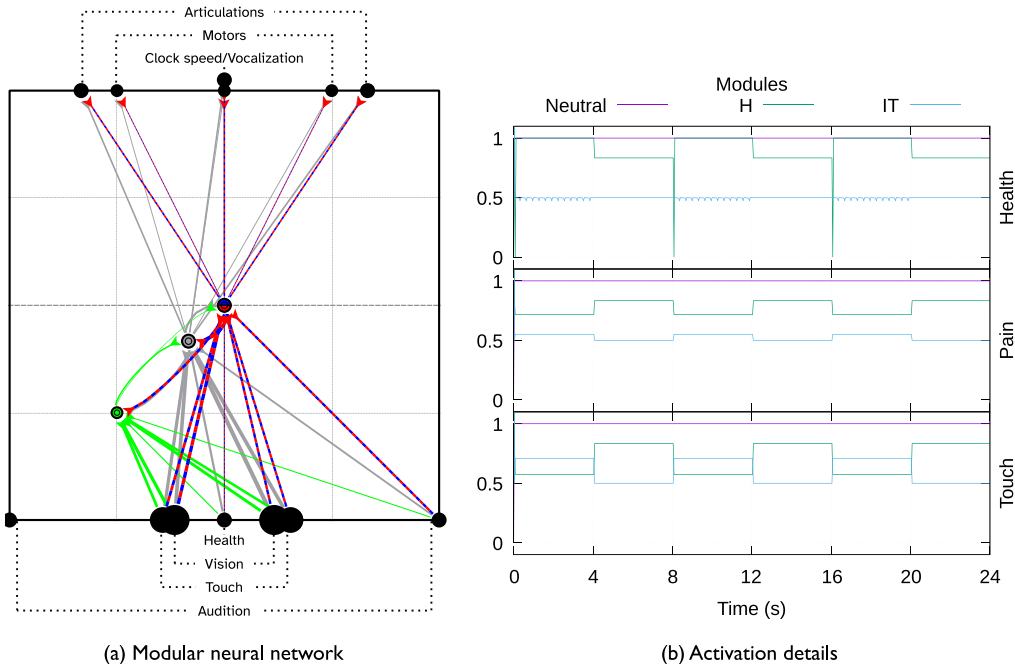


Figure 10. Modular response to elementary stimuli in control conditions. (a) The modular neural network showing the Neutral (gray) and Health (green) modules. The bi-module (red/blue) processes both Touch and Pain information. For more readability, similar inputs and outputs are also aggregated (black). (b) The activity of all modules when in presence and absence of a given stimulus show marked variations depending on the type of the module.

Some trends can be observed by the distribution of clusters across the different types of evolution. Indeed, T2P2, previously found to have four times as many failed runs as any other type, is also fairing poorly from this point of view. It has consistently fewer clustered champions for all stimuli, although by a relatively thin margin. Oppositely, both T1P2 and T2P3, the extremes in terms of environmental complexity, produced more clustered champions, especially with respect to Pain. A similar dynamic can be gathered from Table 3(b), with only a single individual in T2P2 exhibiting all three module types as opposed to the 10 of T1P2. All in all, this differential processing of our stereotypical stimuli seems to have a lower impact than expected across the whole population.

Nevertheless, for those individuals that did respond, we can gather high-level neural dynamics and topologies as illustrated in Figure 10. This champion has a small number of hidden neurons partitioned among a Health module (neurons that responded to stimulus H), a Touch-Pain bi-module (responding to both I and T), and a Neutral module comprising the remaining non-response-specific neurons. Furthermore, we can see that topological and spatial distributions are not equal across the different modules with Touch-Pain lying perfectly at the center of the projected substrate. This implies that the neurons it is composed of are symmetrically placed, as opposed to the Health module, which is focused on the lower left quadrant. In terms of connections, we can see a similar trend with all three modules having different positions in the topology.

Indeed, while all modules collect inputs from all but the left ear, not all have a direct impact on the outputs: the Health module is only connected recurrently to its pairs. In Figure 10(b), we can see the individual module response to the various elementary stimuli with Neutral staying constant throughout the evaluations. Depending on the type of event, however, the remainder exhibit diverging dynamics with, as expected, Health reacting to stimulus H. Of special interest in the drastic response shown when transitioning from full-health to near-death (steps 0, 200, 400). Conversely,

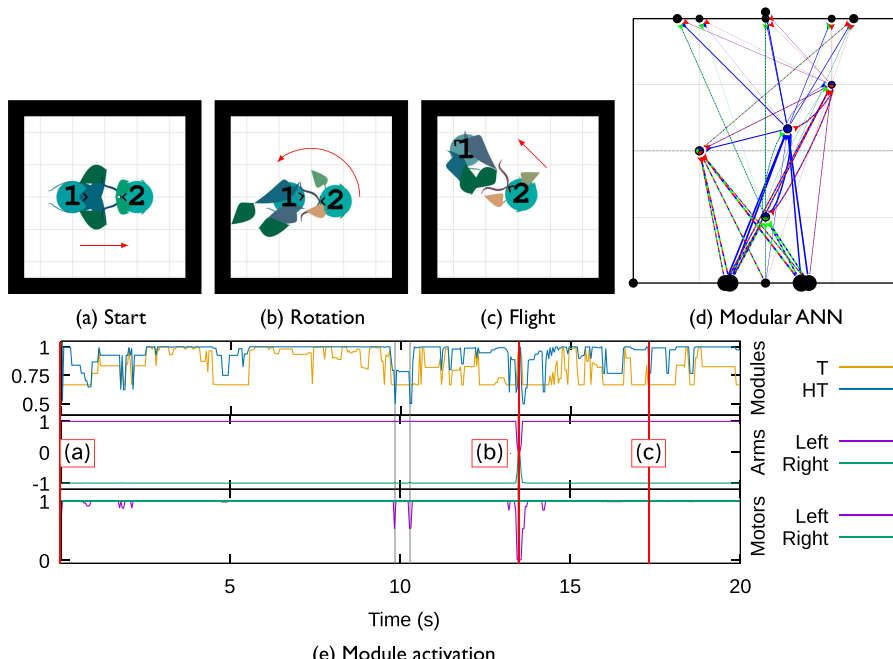


Figure 11. Impact of external events on the high-level dynamics of an ANN. (a) to (c) Illustrations of the creature's strategy: An aggressive charge is followed by a brave flight. (d) The modular neural network shows a solitary single-stimulus module (blue) processing Touch information. Two bi-modules (red/blue and green/blue) aggregate pairs of stimulus, whereas the tri-module (red/green/blue) processes all stimuli at once. (e) Module dynamics with the corresponding three events, highlighted: One too many impacts causes short but significant changes in the state of HT leading to choosing flight over fight.

we can see both modules acting in concert due their recurrent relationship when faced with the other types of stimulus.

It follows that this individual does process different types of “tactile” perceptions despite the limited size of its neural network. One crucial element to consider, however, is that when faced with its “natural” conditions, that is, when fighting its two opponents, the individual manages to never be hit on its main body. Thus, it experiences none of the currently tested stimuli *in the last generation*, thereby preventing its detection by this modularization procedure. This goes to show the advantage of the controlled conditions not only to attenuate input noise but also to extract no longer applicable functional partitions.

Besides this illustration in canonical circumstances, we now turn our attention to the primordial objective: gaining insights into the neuronal implementation of various internal states. As a practical case, in Figure 11, we show an individual with more complex dynamics. Unlike the previous example, all neurons were assigned to a cluster with uneven allocations to the different stimuli. By monitoring the dynamics of a subset of the creature’s modular network, we observe multiple relaxations especially in the Health-Touch (HT) module. The third major one (below 0.6) leads to a drastic change in the outputs HT is connected to: the left motor and elbow articulations. This, in turn, impacts its velocity and triggers a rotation that, when outputs level back to their traditional values, allows the creature to flee. Since the evolutionary fitness penalizes death much more strongly than near-death (Equation 6), this adaptive behavior minimizes loss.

5.2 Evaluation 2: Discrimination

Our second focal point concerned visual inputs and, most importantly, discriminative capabilities. In this case, the stimuli are of larger magnitude than in the first evaluation as we place the subject in front of another individual. The genome used to generate this individual indicates the type of stimulus tested, as summarized in Table 4. Once more three cases are investigated but not all can be applied to a given individual. Indeed, while stimulus B tests for recognition of the opponent, the other two cases are not relevant in all evolution types. The capacity to discriminate between friends and foes, tested in part via stimulus A, only makes sense for tag-team evolutions where there was an ally to identify. Similarly, differentiating between opponents (stimulus C) is only used for cases where there is no single opponent, namely with three co-evolving populations. Thus not all champions are equal in the face of this evaluation, although it suffers from much less observer bias as gaining or losing sight of an individual is not an implausible occurrence.

It follows that, as shown in Table 5, numerous stimuli are not applied to whole slices of the population with only T2P3 being subjected to the full range. Nonetheless, we observe a much stronger response compared to the previous set of stimuli with the lowest frequency at 50% for stimulus C in the T1P3 evolution type. The trend is further confirmed by looking at whether or not individuals’ brains exhibited multiple types of clusters with only a marginally lower minimum.

Table 4. Stimuli applied to an individual in the second type of evaluation.

Type	Name	Applied
B	1st Opponent	all
A	Ally	T2P*
C	2nd Opponent	T*P3

Note. Stimulus B consists in alternating between the previously fought opponent and an empty environment. A and C are not applicable to all individuals as they concern either tag-team evolution (T2P2, T2P3) or three co-evolving populations (T1P3, T2P3).

Table 5. Proportion of champions, in each run type, that exhibited discriminative capabilities.

Type	A	B	C	Type	I+	2+	3
TIP2	–	60.42	–	TIP2	60.42	–	–
TIP3	–	52.08	50.00	TIP3	56.25	45.83	–
T2P2	56.25	52.08	–	T2P2	58.33	50.00	–
T2P3	52.08	54.17	56.25	T2P3	58.33	54.17	50.00

(a) Stimulus specific

(b) Multimodular

Note. Response is higher than previously. Not all stimuli are applicable to all run types indicated by – in corresponding cells. (a) Among the applicable stimuli, more than half of each subpopulation showed positive response with no obvious differences. (b) Multimodularity is drastically more frequent despite reduced opportunities.

In this case, T2P2 comes out in better position although we stress once more that the heterogeneous range of applicable stimuli makes exhaustive comparisons moot.

Rather, we consider Figure 12 depicting dynamics of an individual produced by T2P2. As such, only Ally and 1st Opponent modules can be detected, due to its evolutionary history. In practice,

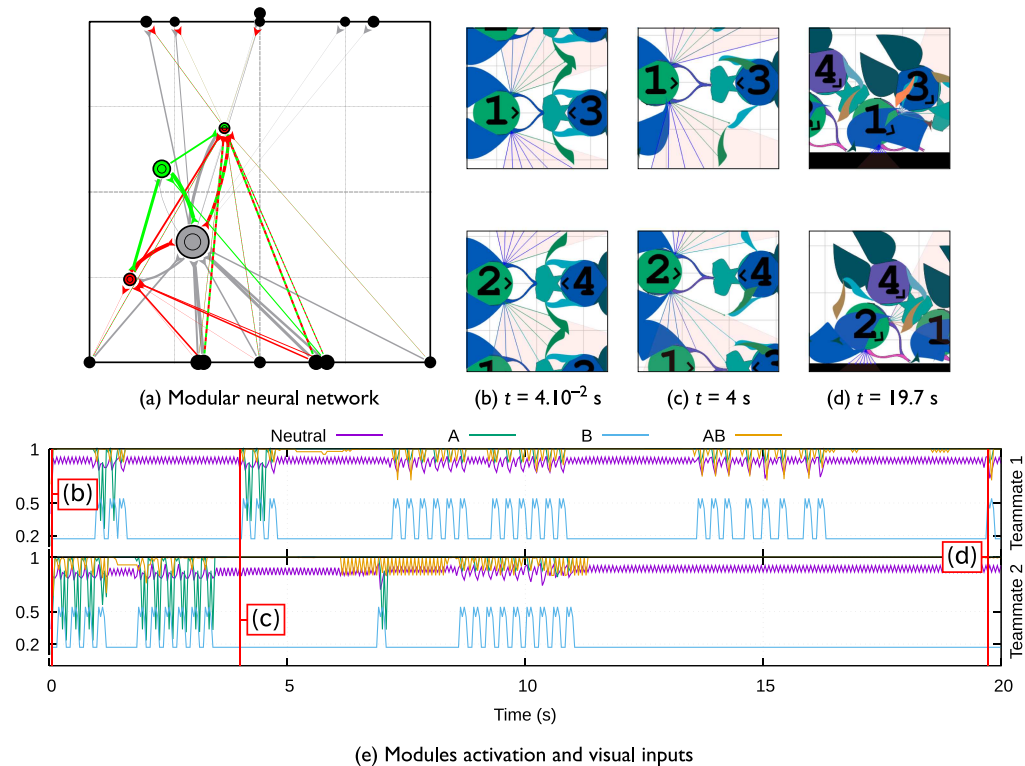


Figure 12. Emergent range-finding. (a) All types of modules are present: Ally (red), Opponent (green), and a bi-modal (red/green). (b) and (e) Different initial internal states depending on the relative enemy position. Individual 2 has 3 visual rays touching the opponent's forearm resulting in a heightened activity. (c) and (e) When situations are reversed, with 1 seeing enough of its opponent's forearm and 2 seeing other types of splines, so are the modules' activity. (d) and (e) Partial detection events, such as the opponent's main body, result in partial modular activation.

Table 6. Stimuli applied to an individual in the third type of evaluation.

Type	Name	Requires
N	Noise	\emptyset
F	Friend	Talkative individual
O	Opponent	One talkative opponent

Note. Stimulus N consists in injecting noise into both of the subject's ears. Stimuli F and O are only applicable when the corresponding agent (ally/opponent) is talkative.

both module types are found with non-trivial densities,⁹ including a bi-modal cluster in the top left quadrant. Surprisingly, its topology is strongly biased toward the left region of the substrate, most clearly so for the Ally module. As with the previous individual, not all inputs/outputs are treated equally across the various modules allowing differential responses to appropriate stimuli as illustrated in Figure 12(e).

Right from the start, both individuals have drastically different action levels across all but the Neutral module. We can link this difference in states to differences in their visual inputs: 1 is located on the bottom of the arena and its right retina mostly sees the boundary (blue). However, in the visual field of individual 2, its direct opponent's forearm, of distinctively green color, occupies exactly three retina cells. This pattern holds true throughout the simulation as indicated in the following set of images, with the roles now inverted. Correlating retina coverage with neural activity allows this individual to perform the non-trivial task of range finding. It compares the projected size of one of its opponent's most troublesome morphological components with an arbitrary threshold to control a subsequent change in regime. It is noteworthy to notice that the pattern also works in other cases, as shown in the last pictures, this time for detecting the opponent's main body. In this case, the reaction is not as strongly marked especially in the Ally module, which remains quiescent. Thus, by combining topological biases with historical knowledge of its enemy, this individual is capable of computing elaborate high-level perceptions from simple RGB components.

5.3 Evaluation 3: Communication

Our final point of inquiry concerns the capacity to process surrounding sounds. As previously, we investigate three types of stimuli, summarized in Table 6, by directly injecting specific frequencies into both of the subject's ears, at maximal volume. The stimulus indicates, in part, the frequency to use with the most trivial case N simply consisting in emitting on the Noise channel. Thus the individual's perception will match that of a rapidly moving object, close by. In both other types of stimuli, we use one of the communication channels, with conditions. For F, the creature must have exhibited vocal behavior while fighting its assigned opponents. The most frequently used channel is then used as input in the evaluation, in the same manner as for N. A similar approach determines the preferred channel of the opponent, this time considering the most vocal opponent for P3 evolution types. Whenever both the opponent and the ally share the same preferred channel, only stimulus F is evaluated. Although this does not mimic the potentially intricate dynamics of every inter-individual communication, the solution is simple enough not to cause excessive biases.

Indeed when considering the frequent distribution of each co-evolving population (Figure 13), we see that, on average, mute individuals are excessively frequent (from 22% to 33%). Additionally, it is also quite clear that most communicate on channel 2 (neural output in $] \frac{1}{3}, 1]$). Thus the number of clearly differentiated soundscapes is relatively low, even more so for T1P2 with only three such

⁹ 31 and 16 neurons in the Opponent and Ally modules, respectively. This figure is out of a total of 113 neurons, that is about 20% of the maximal density.

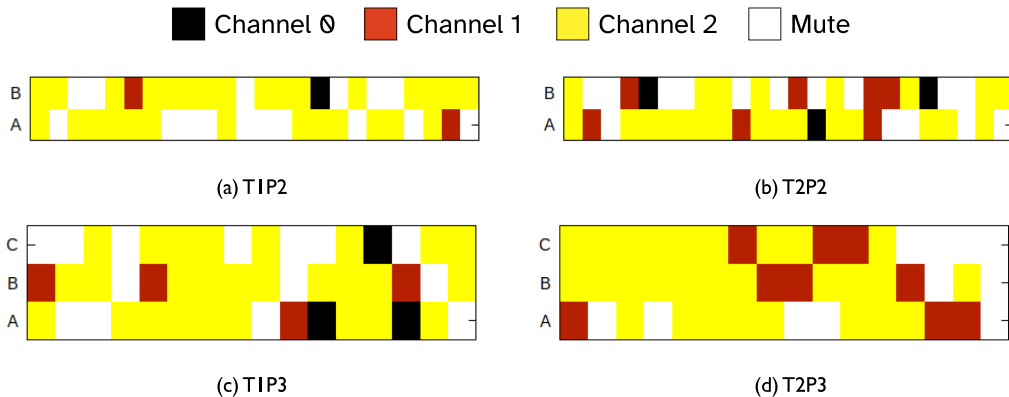


Figure 13. Soundscapes emergence in response to more complex environmental conditions. For each column, the preferred communication channel of each individual is displayed. Despite the reduced number of replicates, runs with three co-evolving populations show markedly more talkativeness and frequential distribution.

Table 7. Proportion of champions, in each run type, that exhibited reaction to auditory cues.

Type	Opp	Friend	Noise	Type	I+	2+	3
TIP2	16.67	29.17	35.42	TIP2	50.00	27.08	4.17
TIP3	8.33	22.92	29.17	TIP3	39.58	18.75	2.08
T2P2	22.92	27.08	35.42	T2P2	52.08	27.08	6.25
T2P3	6.25	18.75	22.92	T2P3	35.42	10.42	2.08

(a) Stimulus specific

(b) Multimodal

Note. (a) Uneven access to stimuli O and F results in drastically reduced response rates. Trends depend both on the type of run and stimulus. (b) Multimodal individuals are at the lowest observed frequency.

cases. The other types do not fare much better with four and five occurrences for types T2P2 and T1P3, respectively. Interestingly, while no individual used channel 0 preferentially in T2P3, exactly 50% of this type of run results in frequently distributed vocalization.

As one can expect, this results in drastically reduced response rates across both O and F stimuli (Table 7). Compared to the other evaluation scenarios, auditory modules are more infrequently detected, inducing fewer multimodal individuals. This time around, we can note that the trend is in favor of P2 evolution types especially for T2P2 which, up until now, tended to score the lowest.

By observing the dynamics of one particular champion from T2P2, we have a small sample of their potential complexity.¹⁰ Figure 14(a) shows the modules (top two rows) and vocal patterns (bottom rows) of a team of two identical individuals. To better understand the acoustic environment they are placed in, we also show the auditory inputs of the first individual for the left ear only (Figure 14(b)). Similar inputs are received by both ears of both individuals with minor differences in magnitude due to varying inter-individual distances. This champion is also the individual with the highest number of hidden neurons across all run types (340). Accordingly numerous neurons show positive response to the modularization procedure (33, 23, and 50 for stimuli O, F, and N, respectively).

10 <https://vimeo.com/godinduboisalife/mk-8167B-communication>.

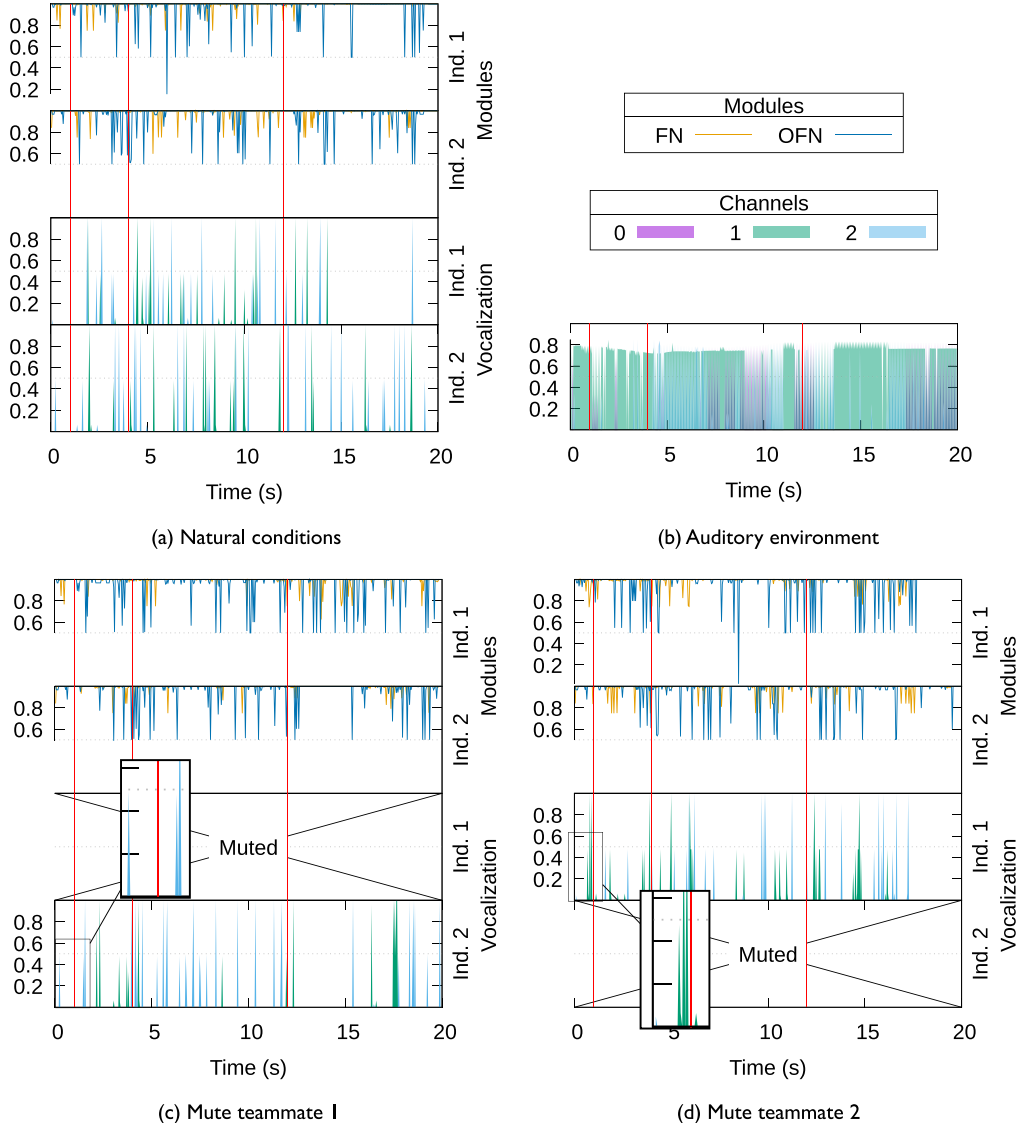


Figure 14. Interaction between modules, vocalization, and environment. (a) In base conditions both individuals communicate via impulses on channels 1 and 2 (bottom rows). Two modules are shown: one biomodal processing Friend and Noise stimuli (FN) and the trimodal (OFN). All have similar spiking pattern in both individuals. (b) They inhabit a very noisy environment due to an extremely talkative opposing team. (c) When muting the first teammate, the vocal response of its partner changes with next-to-no emissions on channel 1. (d) When the second teammate is muted, we can track the difference all the way to the first chirp. This causes opposite activations in both modules of the first teammate, which then performs a strong query.

Strikingly, we can see that sound emission is much sparser than reception with both studied individuals making parsimonious use of channels 1 and 2. Oppositely, the opponents are consistently more vocal across all three channels, thereby polluting the soundscape. However, despite this surrounding noise, both subjects seem engaged in a structured exchange via spikes emitted on alternating channels. In terms of modular activity, we only monitor two specific submodules: Friend-Noise (FN), composed of the neurons found responsive to stimuli N and F, and the tri-module OFN. These exhibit a similar spiking trend, albeit in the downward direction, thereby being more akin to relaxation rather than excitation events.

To better understand the relationship among received auditory cues, modular activity, and behavior, we perform two alternate evaluations with one of the teammates being muted. Thus in Figure 14(c) only the second subject is capable of speaking, all other things being equal. We can see a moderate response to this unexpected silence between time steps 25 and 100 (first two red bars, from 1 s to 4 s). This results in different patterns both vocally and neurally. In the former case, spikes have different timing, magnitude, and channel of emission during this second period and persisting until the end of the evaluation. In the latter case, we can observe a similar trend with a much more sparsely relaxed OFN module. Most interestingly, this selective muteness induces behavioral changes as, in this case, individual 1 fails to acquire its intended target and derives away from its teammate (not shown here).

When inverting the mute/listener role, we obtain a clearer picture in terms of relative dependency. Indeed the first “message” is emitted by individual 2, during the first second (magnified in Figure 14(c)). As can be seen, failure to receive this message causes individual 1 to vocalize repetitively on the opposite channel (magnified in Figure 14(d)). This can be linked to differential activation in the creature’s FN module, which, in the base case, spikes shortly after reception. With a mute teammate, however, this spike occurs later on, triggering the vocalization and, instead, module OFN is the one activating in the first half second.

Again, the pattern produced is much different from the original with frequent spike bursts on channel 1. Modular activity is just as affected with OFN strongly changing regime at two places instead of the more uniform behavior observed in the base case. However, in this case, functional behavior seems less affected as both individuals manage to attack the same target. Comparing the impact of all three cases hints at communication serving a coordination purpose that turns out to be crucial, at least for the first teammate.

6 Meta-Modularity

The various stimuli each creature has been subjected to can be broadly classified by the “sense” they call upon. Indeed I (Pain), H (Healthiness), and T (Touch) should trigger reactions in neurons responsible for the well-being of the creature. Similar reasoning can be done for the other triplets with A (conspecific), B (1st opponent), C (2nd opponent) highlighting visually active brain regions and N, F, O auditory areas.

Thus by aggregating these various stimuli as the partition suggests, we can extract a higher-level map of a creature’s ANN: a “cognitive” map of sorts. This allows for a more complete look at the neural implementation of the various senses with respect to their interaction with the inputs/outputs and with one another. Such a procedure has been applied to the individuals previously presented in this study, as shown in Figure 15 with varying degrees of complexity. On one end of the spectrum, ANNs with a limited number of hidden neurons are poorly suited to further clustering. For instance,

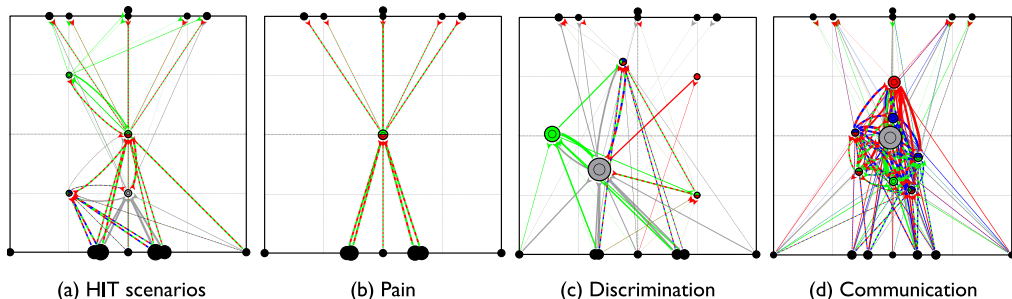


Figure 15. Mapping stimulus-specific modules to senses. Brain regions aggregated by type of stimulus: red, green, and blue correspond to pain, visual, and auditory modularizations. The networks presented correspond to the previously investigated individuals. Some ((a) and (b)) show sparse repartitions of the different areas while (d) averages out at the center.

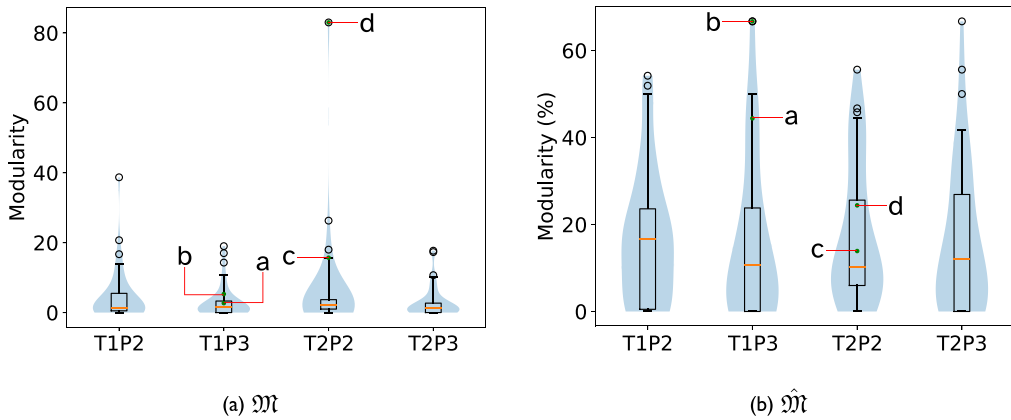


Figure 16. Distribution of “cognitive” capabilities by run type. No type is significantly more efficient at promoting modularity. Individuals from Figure 15(a), (b), (c), and (d) are highlighted here as a, b, c, and d.

the creature in Figure 15(b) only seems to react to two senses (Touch and Vision) but does so with all of its eight hidden neurons. On the other side of the spectrum, the communicating champion of the previous section (shown in Figure 15(d)) has enough neurons to allow for extensive partitioning and, indeed a large number of neurons remains unassigned. However, whether these process untested types of stimuli or serve more generic purposes is unclear. A better spatial distribution is shown for the other two showcased individuals (in Figure 15(a) and Figure 15(c)) with clearly separated regions dedicated to the various senses.

To characterize this subdivision of an ANN into stimuli-specific subsets, we define two modularity metrics:

$$\mathfrak{M} = \frac{1}{3}(|T| + |V| + |A|) + \frac{2}{3}(|TV| + |TA| + |VA|) + |TVA| \quad (9)$$

where $|T|, |V|, |A|$ are the sizes of the *meta-module* associated with tactile, visual, and auditory information, respectively. Similarly, $|TV|, |TA|, |VA|$ are the sizes of the meta-modules processing two senses and $|TVA|$ that of the tripotent. Informally, \mathfrak{M} measures the average cognitive investment across all three senses and favors generalist networks. However, as it is heavily correlated with the size of the ANN, we also consider its normalized version:

$$\hat{\mathfrak{M}} = \frac{\mathfrak{M}}{|H|} \quad (10)$$

where $|H|$ is the number of hidden neurons. In this case, the bias is reverted with small networks being favored as a single hidden neuron assigned to the TVA meta-module would result in a score of 100%.

When applying both metrics to the 192 champions (Figure 16), we see similar distributions across the different evolutionary protocols with no statistical differences detected.¹¹ As a matter of fact, as no *explicit* evolutionary pressure was put on the emergence of modularity, all groups performed fairly well with only 23%¹² of neural networks exhibiting no such capacity. Furthermore, observing the relative ordering of the previously presented individuals with respect to both metrics paints a different picture of how they approached modularity. (See Figure 16, which highlights the individuals shown in Figure 15(a), (b), (c), and (d) as a, b, c, d.) Indeed individuals a and b are

¹¹ One-sided Mann-Whitney test, all p values > 0.025 .

¹² T1P2: 23.4%, T2P2: 13.6%, T1P3: 29.8%, T2P3: 27.6%.

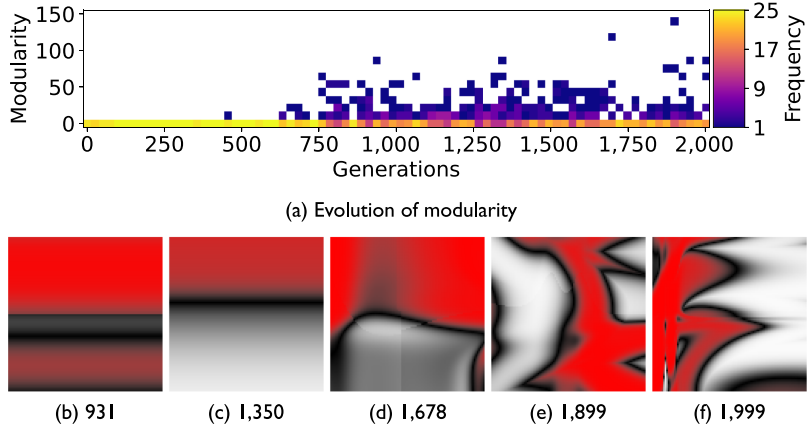


Figure 17. Evolutionary dynamics of modularity \mathfrak{M} over time for the individual from Figure 15(d). (a) While the progression is far from monotonous, an upward trend is observable starting around generation 650. (b) and (c) Samples of the CPPN output exhibiting simple partitioning of input types. The pattern is produced by querying for $(u, -1, v)$ and $(0, 0, 0)$. (d) to (f) More complex anisotropic patterns emerge in latter generations.

representative of small, fully differentiated neural networks, with a correspondingly high score in $\hat{\mathfrak{M}}$. Oppositely, both c and d are markedly larger with a non-trivial number of unassigned hidden neurons.

Additionally, the metric \mathfrak{M} makes it possible to track the evolution of modularity across the generations as shown in Figure 17 for the communicative champion. While initially scoring very low, by the 750th generation mark, the first highly modular neural networks start to emerge. However, due to the multiple subpopulations mentioned in the morphological section, the process is far from monotonous: It fluctuates widely depending on the dominant lineage and the opponents' characteristics. Nonetheless, there is a noticeable increase in complexity as outliers reach ever upward.

We can relate such progress to the cumulative refinement of the underlying CPPNs and, more specifically, to the processing of the various inputs. To this end, the lower panels of the same figure (Figure 17(b) to 17(f)) show the weight output at various key points of the evolution. The image is produced by varying coordinates x_0, z_0 while keeping all others fixed: $y_0 = -1$ and $x_1 = y_1 = z_1 = 0$. This way the outgoing connectivity pattern can be observed for potential neurons on the input layer with the magnitude expressed on a red-black-white color scale. From this, we can observe that, initially, there is a partitioning between the different types of inputs most visible in Figure 17(b). In this case, the various bands observed seem to closely reproduce the position of the input neurons.¹³ However, in later generations, this pattern becomes more intricate with none of these types of clear-cut distributions. Indeed, given the complexity of, for example, Figure 17(f) across as low as two dimensions, the amount of information contained by the CPPN, when taking into consideration all six of them as well as the three output types, is of staggering proportions.

However, not all populations have focused on modularity with the same intensity as illustrated with the evolutionary dynamics of Figure 18. Indeed, while individual c (from Figure 15(c)) displays better-than-average values for both \mathfrak{M} and $\hat{\mathfrak{M}}$, its trend across time is more akin to multiple nonpersistant progressions rather than a continuous process. At the other end of the spectrum, individuals with a limited number of hidden neurons such as individual a from Figure 15(a) exhibit only punctual modular response.

Thus by building upon the detection of responses to elementary stimuli, we can extract a higher-level map of an arbitrary ANN with respect to its topology. Such an overview of the creature's "cognitive maps" is helpful in highlighting the proportional allocation of neural resources

¹³ $z > 0$ for retinal neurons, $z \in [-1/8, 1/8]$ for tactile.

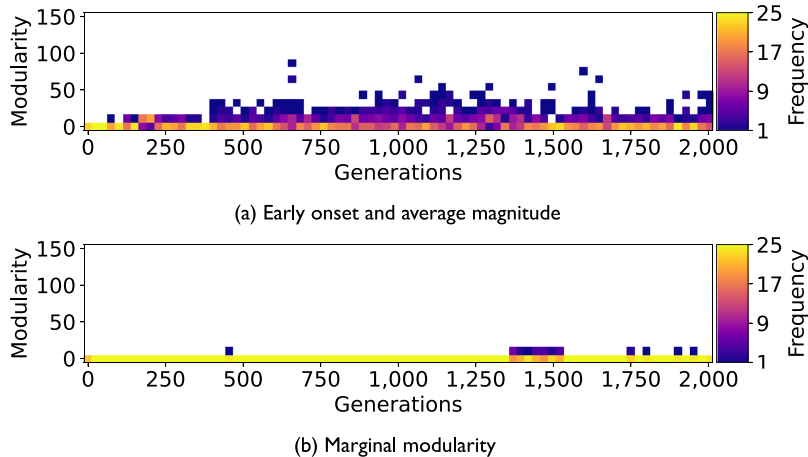


Figure 18. Complementary evolutionary dynamics of modularity \mathfrak{M} . (a) Individual from Figure 15(c) discovers modularity in the first hundred generations but the magnitude and progress are less pronounced. (b) Individual from Figure 15(a) illustrates runs where modular structuration is never a predominant concern.

and its dynamics across evolution. Indeed, this approach to functional, bottom-up detection of hierarchical structures in an unbiased neural substrate shows promising capabilities to jointly address connectivist and explainable AI.

7 Conclusion

In this article we presented an implementation of ES-HyperNEAT in grounded artificial creatures (Splinooids) that engaged in individual and team competitions. These creatures have numerous morphological components from the position of their eyes to spline-based structures that serve both defensive and offensive purposes. Similarly, part of their neural input was evolving in response to perceived environmental constraints, most notably their retina cell density and the relative position of their touch sensors. Furthermore, they were interacting with the environment in an atomic manner via rotational motors and frequency-based vocalization. This was tied into an implementation of physical confrontation via inertia transfer and differential densities, allowing the individuals to evolve a variety of viable strategies. When they were deployed in a co-evolutionary experiment with a differing number of teammates and confronted populations, we observed diverse morphological and behavioral strategies (e.g., frontal confrontation, evasive, boxer). Despite not producing more massive ANNs, evolution types with more complex conditions were found to result in more aggressive competitors, scoring significantly more hits.

Most importantly, however, monitoring the differential activation of each individual's neurons in canonical scenarios made it possible to observe functional clustering of the creatures' brains. More specifically, we investigated three types of reactions: pain, vision, and audition, each with varying response levels but consistent across all evolution types. It was found that the resulting creatures did exhibit functional neural partitioning with some processing touch, to switch from fight to flight behavior, while others discovered range-finding via retina input saturation. Furthermore, we detailed the vocal behavior of a non-trivially communicating team linking specific auditory events to internal states in spite of an extremely noisy environment. The main contribution, however, is that these analyses were guided by the modular ANN extracted through an fMRI-like procedure. In this manner, we were able to observe the neural dynamics of the creatures via specific functional prisms, thereby improving the explainability of connectivist ANNs. Furthermore, we introduced a potential extension of this method through hierarchical clustering to combine stimulus-specific clusters into higher-level behavioral modules. In large neural networks, this would further help to extract

mapping of an arbitrary creature's brain into useable cognitive models to monitor its activity or evolutionary history.

Future investigations could focus on other aspects of both this experiment and the model in general. One crucial point that is left unaddressed in this article is the question of physical clustering as, currently, modules can be composed of distant neurons. Similarly, most ANNs only reach a processing depth of 3, meaning that a neuron is only three steps removed from the inputs precluding the emergence of long processing pipelines. Finally, in terms of experiments two future directions can be envisaged: extending the team-based competition and further exploring communication. In the former case, we plan on moving onto heterogeneous teams instead of using clones, which would allow for more diverse strategies such as division of labor. The latter case would leverage results observed in the last type of evaluation where structured noise-resistant communication spontaneously emerged. Further exploration of the vocal capabilities of neuroevolving creatures could prove instrumental not only in understanding its mechanisms in primitive animals but also to potentially reach self-explainable AI.

Acknowledgments

This work was granted access to the HPC resources of CALMIP supercomputing center (allocation P16043).

References

- Aaltonen, T., Adelman, J., Akimoto, T., Albrow, M. G., Alvarez González, B., Amerio, S., Amidei, D., Anastassov, A., Annovi, A., Antos, J., Apollinari, G., Apresyan, A., Arisawa, T., Artikov, A., Ashmanskas, W., Attal, A., Aurisano, A., Azfar, F., Azzurri, P., ... Zucchelli, S. (2009). Measurement of the top-quark mass with dilepton events selected using neuroevolution at CDF. *Physical Review Letters*, 102(15), Article 152001. <https://doi.org/10.1103/PhysRevLett.102.152001>, PubMed: 19518620
- Broekens, J., Jacobs, E., & Jonker, C. M. (2015). A reinforcement learning model of joy, distress, hope and fear. *Connection Science*, 27(3), 215–233. <https://doi.org/10.1080/09540091.2015.1031081>
- Chen, K., Hwu, T., Kashyap, H. J., Krichmar, J. L., Stewart, K., Xing, J., & Zou, X. (2020). Neurorobots as a means toward neuroethology and explainable AI. *Frontiers in Neurorobotics*, 14, Article 570308. <https://doi.org/10.3389/fnbot.2020.570308>, PubMed: 33192435
- Cliff, D., & Miller, G. F. (1996). Co-evolution of pursuit and evasion II: Simulation methods and results. In P. Maes, M. J. Mataric, J.-A. Meyer, J. Pollack, & S. W. Wilson (Eds.), *From animals to animats 4: Proceedings of the fourth international conference on simulation of adaptive behavior* (pp. 506–516). MIT Press. <https://doi.org/10.7551/mitpress/3118.003.0061>
- de Freitas, J. S., Imbert, R., & Queiroz, J. (2007). Modeling emotion-influenced social behavior for intelligent virtual agents. In A. Gelbukh, & Á. F. Kuri Morales (Eds.), *MICAI 2007: Advances in artificial intelligence* (LNCS 4827, pp. 370–380). Springer. https://doi.org/10.1007/978-3-540-76631-5_35
- Delgado-Mata, C., Martínez, J. I., Bee, S., Ruiz-Rodarte, R., & Aylett, R. (2007). On the use of virtual animals with artificial fear in virtual environments. *New Generation Computing*, 25(2), 145–169. <https://doi.org/10.1007/s00354-007-0009-5>
- Ellefse, K. O., Mouret, J.-B., & Clune, J. (2015). Neural modularity helps organisms evolve to learn new skills without forgetting old skills. *PLOS Computational Biology*, 11(4), Article e1004128. <https://doi.org/10.1371/journal.pcbi.1004128>, PubMed: 25837826
- Godin-Dubois, K., Cussat-Blanc, S., & Duthen, Y. (2021a). *On the benefits of emergent communication for threat appraisal* [Workshop presentation]. ABMHuB'21: 3rd International Workshop on Agent-Based Modelling of Human Behaviour (Virtual workshop). Available at <http://abmhub.cs.ucl.ac.uk/2021/>
- Godin-Dubois, K., Cussat-Blanc, S., & Duthen, Y. (2021b). Spontaneous modular neuroevolution arising from a life/dinner paradox. In *ALIFE 2021: Proceedings of the 2021 conference on artificial life* (Article 95). MIT Press. https://doi.org/10.1162/isal_a_00431
- Ito, T., Pilat, M. L., Suzuki, R., & Arita, T. (2013). Coevolutionary dynamics caused by asymmetries in predator-prey and morphology-behavior relationships. In *ECAL 2013: The twelfth European conference on artificial life* (pp. 439–445). MIT Press. <https://doi.org/10.7551/978-0-262-31709-2-ch063>

- Jim, K.-C., & Giles, C. L. (2000). Talking helps: Evolving communicating agents for the predator-prey pursuit problem. *Artificial Life*, 6(3), 237–254. <https://doi.org/10.1162/106454600568861>, PubMed: 11224918
- Kadam, S., & Vaidya, V. (2021). Cognitive evaluation of machine learning agents. *Cognitive Systems Research*, 66, 100–121. <https://doi.org/10.1016/j.cogsys.2020.11.003>
- Kadish, D., Risi, S., & Beloff, L. (2019). An artificial life approach to studying niche differentiation in soundscape ecology. In *ALIFE 2019: Proceedings of the 2019 conference on artificial life* (pp. 52–59). MIT Press. https://doi.org/10.1162/isal_a_00140
- Kamilaris, A., & Prenafeta-Boldú, F. X. (2018). Deep learning in agriculture: A survey. *Computers and Electronics in Agriculture*, 147, 70–90. <https://doi.org/10.1016/j.compag.2018.02.016>
- Ledoux, J. (1998). *The emotional brain: The mysterious underpinnings of emotional life*. Simon & Schuster.
- Lotfi, E., & Akbarzadeh-T., M.-R. (2014). Practical emotional neural networks. *Neural Networks*, 59, 61–72. <https://doi.org/10.1016/j.neunet.2014.06.012>, PubMed: 25078111
- Miconi, T. (2008). Evosphere: Evolutionary dynamics in a population of fighting virtual creatures. In *2008 IEEE congress on evolutionary computation* (pp. 3066–3073). IEEE. <https://doi.org/10.1109/CEC.2008.4631212>
- Miconi, T., Clune, J., & Stanley, K. O. (2018). Differentiable plasticity: Training plastic neural networks with backpropagation. In *ICML 2018: Proceedings of the 35th international conference on machine learning* (PMLR 80, pp. 3559–3568). MLR Press. <https://proceedings.mlr.press/v80/miconi18a.html>
- Mnih, V., Kavukcuoglu, K., Silver, D., Rusu, A. A., Veness, J., Bellemare, M. G., Graves, A., Riedmiller, M., Fidjeland, A. K., Ostrovski, G., Petersen, S., Beattie, C., Sadik, A., Antonoglou, I., King, H., Kumaran, D., Wierstra, D., Legg, S., & Hassabis, D. (2015). Human-level control through deep reinforcement learning. *Nature*, 518(7540), 529–533. <https://doi.org/10.1038/nature14236>, PubMed: 25719670
- Moriarty, D. E., & Miikkulainen, R. (1996). Evolving obstacle avoidance behavior in a robot arm. In P. Maes, M. J. Mataric, J.-A. Meyer, J. Pollack, & S. W. Wilson (Eds.), *From animals to animats 4: Proceedings of the fourth international conference on simulation of adaptive behavior* (pp. 468–475). MIT Press. <https://doi.org/10.7551/mitpress/3118.003.0056>
- Mouret, J.-B., & Tonello, P. (2014). Artificial evolution of plastic neural networks: A few key concepts. In T. Kowaliw, N. Bredeche, & R. Doursat (Eds.), *Growing adaptive machines* (pp. 251–261). Springer. https://doi.org/10.1007/978-3-642-55337-0_9
- Olson, R., Hintze, A., Dyer, F., Moore, J., & Adami, C. (2016). Exploring the coevolution of predator and prey morphology and behavior. In *ALIFE 2016: Proceedings of the fifteenth international conference on the synthesis and simulation of living systems* (pp. 250–257). MIT Press. <https://doi.org/10.7551/978-0-262-33936-0-ch045>
- Papavasileiou, E., Cornelis, J., & Jansen, B. (2021). A systematic literature review of the successors of “Neuroevolution of augmenting topologies.” *Evolutionary Computation*, 29(1), 1–73. https://doi.org/10.1162/evco_a_00282, PubMed: 33151100
- Pianca, F., & Santucci, V. G. (2022). Interdependence as the key for an ethical artificial autonomy. *AI & Society*. <https://doi.org/10.1007/s00146-021-01313-x>
- Pichler, P. P., & Cañamero, L. (2008). Evolving morphological and behavioral diversity without predefined behavior primitives. In *ALIFE XI: Proceedings of the 11th international conference on the synthesis and simulation of living systems* (pp. 474–481). MIT Press. Available at <https://archive.org/details/ArtificialLifeXI>
- Reshma, I. A., Cussat-Blanc, S., Ionescu, R. T., Luga, H., & Mothe, J. (2021). Natural vs. balanced distribution in deep learning on whole slide images for cancer detection. In *SAC '21: Proceedings of the 36th annual ACM symposium on applied computing* (pp. 18–25). ACM. <https://doi.org/10.1145/3412841.3441884>
- Risi, S., & Stanley, K. O. (2012). An enhanced hypercube-based encoding for evolving the placement, density, and connectivity of neurons. *Artificial Life*, 18(4), 331–363. https://doi.org/10.1162/ARTL_a_00071, PubMed: 22938563
- Sims, K. (1994). Evolving 3D morphology and behavior by competition. *Artificial Life*, 1(4), 353–372. <https://doi.org/10.1162/artl.1994.1.4.353>
- Stanley, K. O. (2007). Compositional pattern producing networks: A novel abstraction of development. *Genetic Programming and Evolvable Machines*, 8(2), 131–162. <https://doi.org/10.1007/s10710-007-9028-8>

- Stanley, K. O., Bryant, B. D., & Miikkulainen, R. (2005). Evolving neural network agents in the NERO video game. In G. Kendall & S. Lucas (Eds.), *CIG'05: Proceedings of the IEEE symposium on computational intelligence and games* (pp. 182–189). IEEE. Available at <https://citeseerx.ist.psu.edu/viewdoc/download?doi=10.1.1.124.2234&rep=rep1&type=pdf>
- Stanley, K. O., Clune, J., Lehman, J., & Miikkulainen, R. (2019). Designing neural networks through neuroevolution. *Nature Machine Intelligence*, 1(1), 24–35. <https://doi.org/10.1038/s42256-018-0006-z>
- Stanley, K. O., D'Ambrosio, D. B., & Gauci, J. (2009). A hypercube-based encoding for evolving large-scale neural networks. *Artificial Life*, 15(2), 185–212. <https://doi.org/10.1162/artl.2009.15.2.15202>, PubMed: 19199382
- Stanley, K. O., & Miikkulainen, R. (2002). Evolving neural networks through augmenting topologies. *Evolutionary Computation*, 10(2), 99–127. <https://doi.org/10.1162/106365602320169811>, PubMed: 12180173
- Tonelli, P., & Mouret, J.-B. (2013). On the relationships between generative encodings, regularity, and learning abilities when evolving plastic artificial neural networks. *PLOS ONE*, 8(11), Article e79138. <https://doi.org/10.1371/journal.pone.0079138>, PubMed: 24236099
- Treccani, C. (2020). The brain, the artificial neural network and the snake: Why we see what we see. *AI & Society*, 36, 1167–1175. <https://doi.org/10.1007/s00146-020-01065-0>
- Turk, G. (2010). Sticky feet: Evolution in a multi-creature physical simulation. In *Artificial life XII: Proceedings of the 12th international conference on the synthesis and simulation of living systems* (pp. 496–503). MIT Press. Available at <https://archive.org/details/ArtificialLifeXII>
- Verbancsics, P., & Stanley, K. O. (2011). Constraining connectivity to encourage modularity in HyperNEAT. In *GECCO '11: Proceedings of the 13th annual genetic and evolutionary computation conference* (pp. 1483–1490). ACM. <https://doi.org/10.1145/2001576.2001776>
- Witkowski, O., & Ikegami, T. (2016). Emergence of swarming behavior: Foraging agents evolve collective motion based on signaling. *PLOS ONE*, 11(4), Article e0152756. <https://doi.org/10.1371/journal.pone.0152756>, PubMed: 27119340
- Zador, A. M. (2019). A critique of pure learning and what artificial neural networks can learn from animal brains. *Nature Communications*, 10(1), Article 3770. <https://doi.org/10.1038/s41467-019-11786-6>, PubMed: 31434893